Earth and Space Science

Supporting Information for

Estimation of mud and sand fractions and total concentration from coupled optical-acoustic sensors

Duc Tran[1,3], Matthias Jacquet[1], Stuart Pearson[2], Bram Van Prooijen[2], and Romaric Verney[1]

[1] IFREMER, DYNECO/DHYSED, ZI pointe du Diable, CS10070 Plouzane, France

[2] Faculty of Civil Engineering and Geosciences, Delft University of Technology, P.O. Box 5048, 2600GA, Delft, the Netherlands

[3] Current: Royal Belgian Institute of Natural Sciences, OD Nature, Rue Vautier 29, 1000 Brussels, Belgium

Contents of this file

Figures S1 to S31

Introduction

This section provides:

1. Extra information on the particle size distributions of the Bentonite and sands used in this study,
2. A zoom in to ± 10% accuracy of Figure 6 in the manuscript for better visualization,
3. The SCI functions of all the other pairs. In these figures, blue circles or red squares represent data from Q1 or Q2, respectively. Blue or red curves indicate the SCI functions obtained from either Q1 or Q2 data set. The mathematical functions displayed in the sub-figures were obtained from data set Q12 (black line). As discussed in Section 3.2, for pure Bentonite and pure sand conditions only concentration C = 100 mg/L was used to minimized the variations in these two extreme cases. And,

   a note regarding the experimental setup as follows:

   - The DEXMES is a 1 m^3 tank. Thus, even with a low concentration, e.g., 15 mg/L, we still needed a large amount of Bentonite. Due to the amount of Bentonite per run, sonication to bring the Bentonite to primary particle size is impossible. Hence, we used a 5 L beaker and a high speed mixer to mix dry Bentonite with

water. Floc size was not monitored during this step. However, we believe that it is reasonable to make an assumption that by the end of this step, due to 1) very high concentration, 2) long time of mixing and 3) results from previous studies, Tran and Strom (2017, 2018, 2019), the floc size should reach equilibrium.

- The Bentonite from Step 1 (already at equilibrium floc size) now is introduced into the DEXMES tank. The floc size in this step was monitored by a LISST-100X. This 30 minute time step provided enough time for preparation of the next experiment. This included 1) preparing Bentonite (in Step 1 – mentioned above) for the next run, 2) checking and saving data from previous run (we only had two computers to control 6 sensors and the AQUAscat with very large data files that sometimes frozen the computer and required sensors to be restarted, 3) gently and frequently cleaning all the sensors to avoid accumulation of bubbles, and 4) taking water samples and repeating all the steps for the next run.
- The DEXMES tank has a concave, elliptical bed. Once the impeller draws the water towards the bottom, the bed will reflect and generate a jet flow in which the deposited sand is resuspended as much as possible. There are four baffles attached to the inner side of the wall to break the vortexes. Hence, the main stream within the tank goes up the side and then down the centre, recirculating again towards the centre of the DEXMES (please refer to Figure 1). That ensures that the sand can be quickly distributed throughout the tank. The ADV and Wetlab data showed that the signals became stable after about 3-4 minutes. We chose to record the data after 5 minutes to have a homogenous suspension and reduce the deposition of the sand, and to keep the suspended concentration as close to the target as possible.

References:

Tran, D.A., and Strom. K. (2019): Floc sizes and resuspension rates from fresh deposits: Influences of suspended sediment concentration, turbulence, and deposition time. *Estuarine, Coastal and Shelf Science*, 123:6736 - 6752

Tran, D.A., Kuprenas, R., and Strom. K. (2018) How do changes in suspended sediment concentration alone influence the size of mud flocs under steady turbulent shearing? *Continental Shelf Research*, 158:1 - 14

Tran, D.A., and Strom, K. (2017): Suspended clays and silts: Are they independent or dependent fractions when it comes to settling in a turbulent suspension? *Continental Shelf Research*, 138:81 – 94

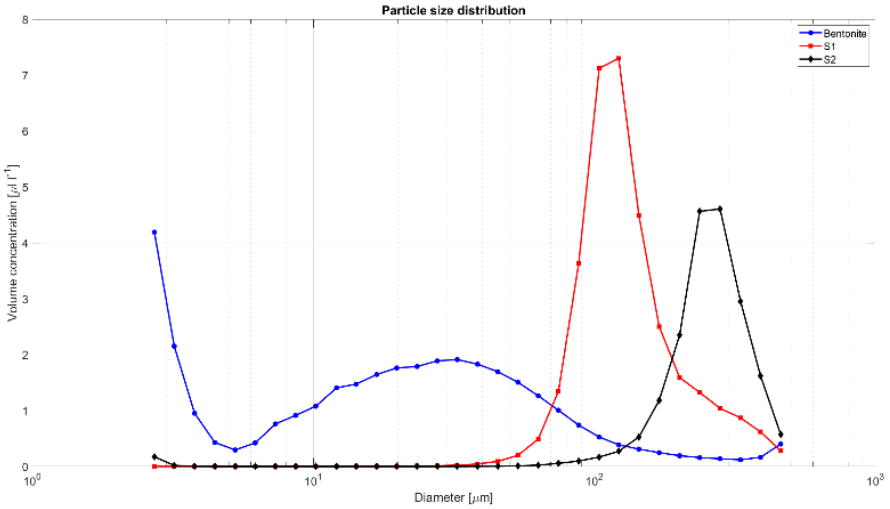

Figure S1. Particle size distributions of Bentonite and sand, S1 and S2 measured by LISST-100X.

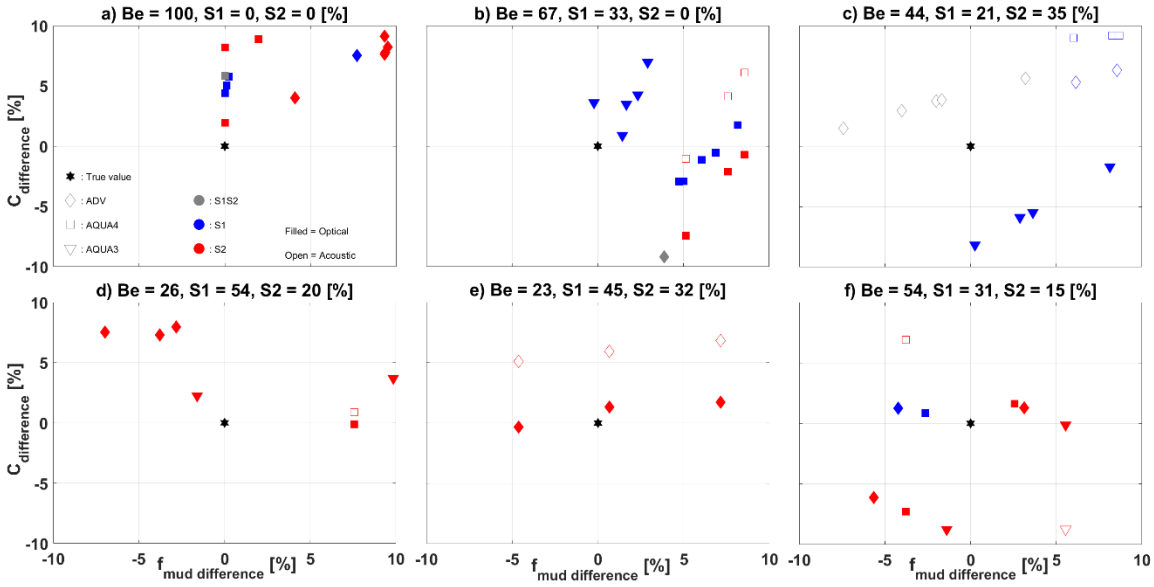

Figure S2. Application of SCI functions, derived from Qset, to Vset data. The sub-figures show results from all pairs of each experimental condition. The legend should be read as a combination of marker + color + filled/open. Where filled marker = Co, empty marker = Ca. For example, a blue-filled diamond means Co was obtained by Q12-(O800->420 – A6) functions. Differences are calculated as Xdifference = (Xestimated - Xmeasured) / Xmeasured * 100%, where X denotes fmud or C. *This figure provide a zoom in a the window of accuracy of ± 10% of Figure 6 in the manuscript.*

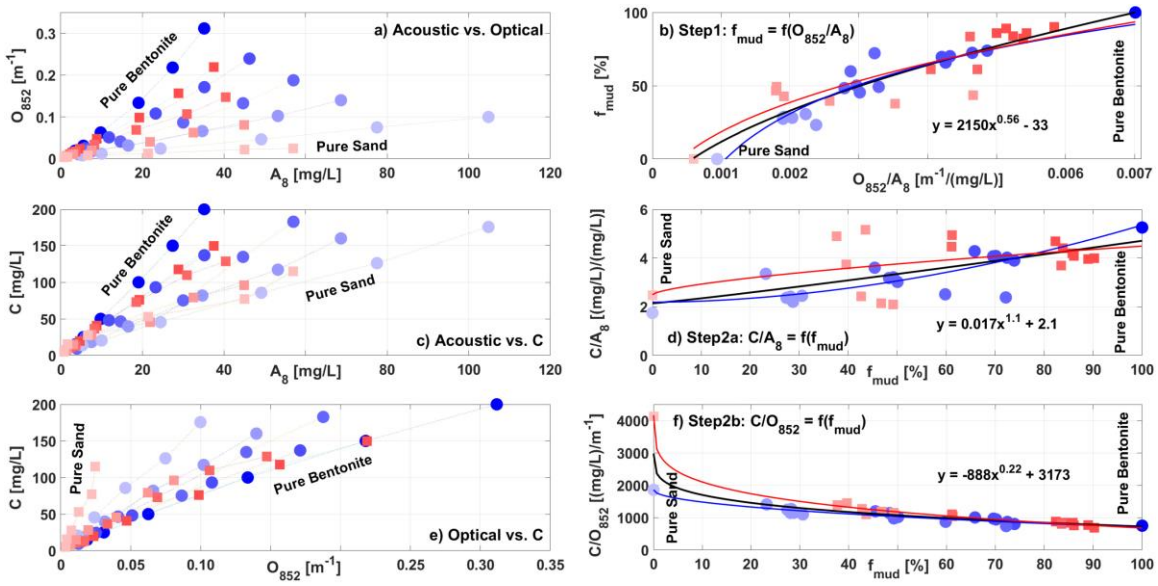

Figure S3. Application of SCI method to the optical/acoustic pair of $\mathbf{O}_{852}$ and $\mathbf{A}_8$ with data in Q1 (blue), Q2 (red), and Q12 (black). The reductions of f_{mud} from 100% to 0% are shown by the darkest color to lightest color. The displayed function are obtained from data set Q12.

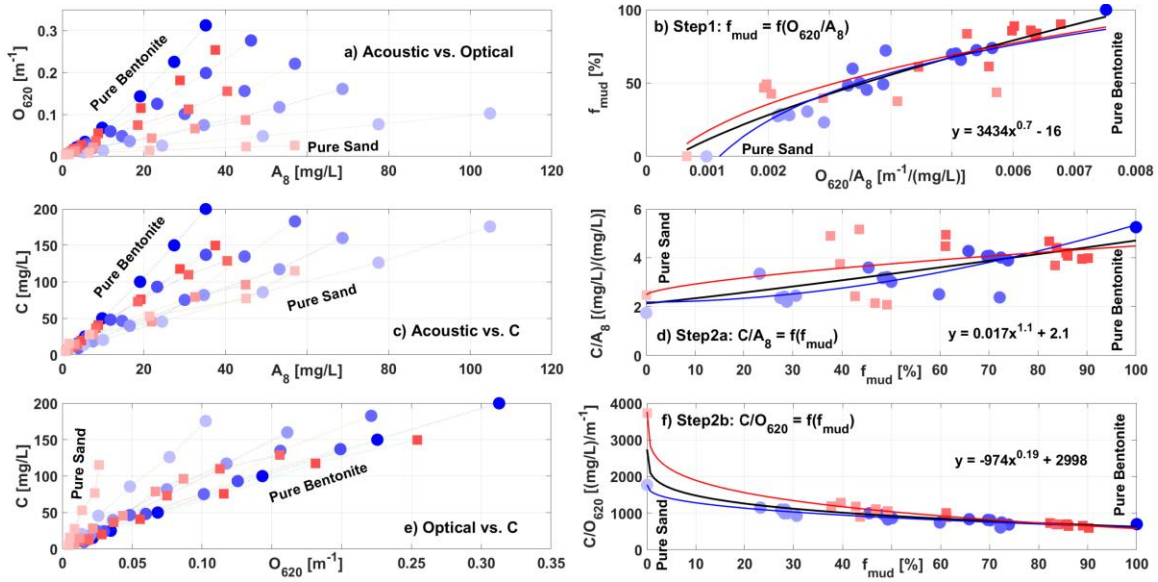

Figure S4. Application of SCI method to the optical/acoustic pair of $\mathbf{O}_{620}$ and $\mathbf{A}_8$ with data in Q1 (blue), Q2 (red), and Q12 (black). The reductions of f_{mud} from 100% to 0% are

shown by the darkest color to lightest color. The displayed function are obtained from data set Q12.

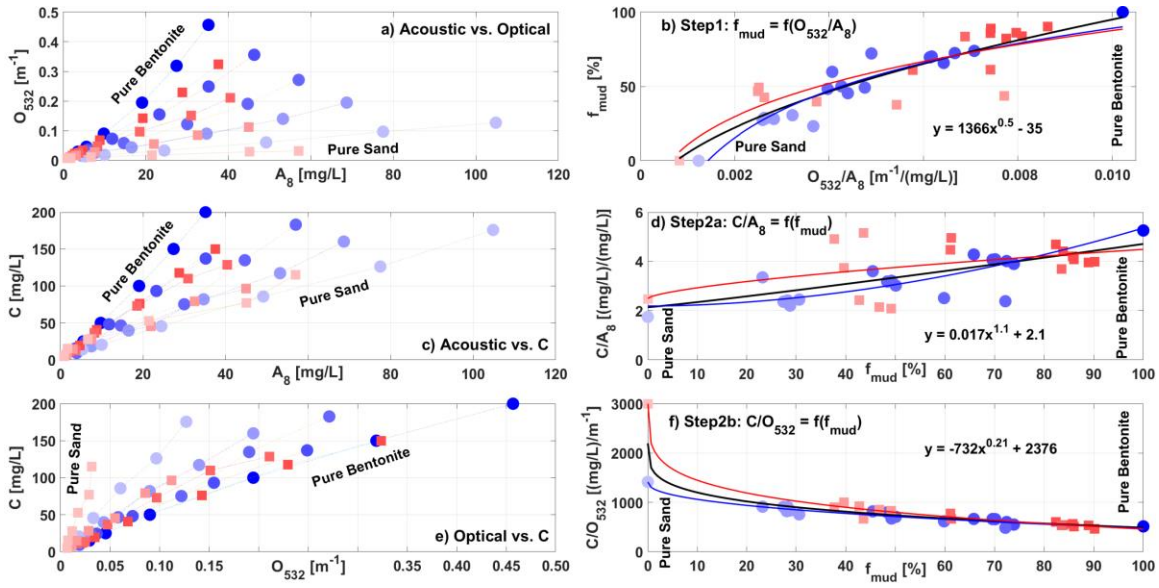

Figure S5. Application of SCI method to the optical/acoustic pair of $\mathbf{O}_{532}$ and $\mathbf{A}_8$ with data in Q1 (blue), Q2 (red), and Q12 (black). The reductions of f_{mud} from 100% to 0% are shown by the darkest color to lightest color. The displayed function are obtained from data set Q12.

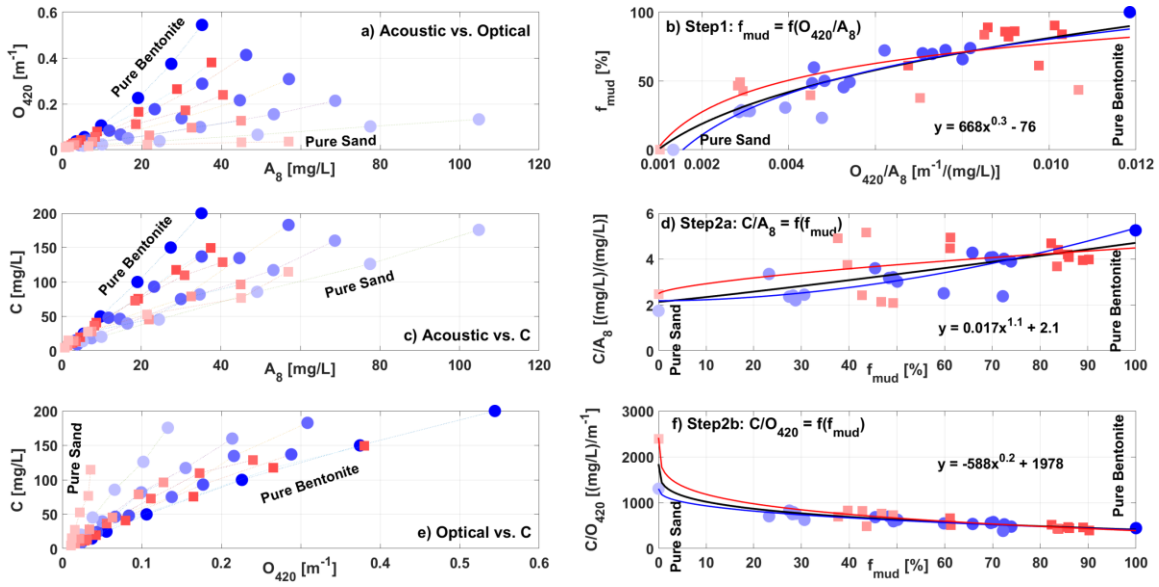

Figure S6. Application of SCI method to the optical/acoustic pair of $\mathbf{O}_{420}$ and $\mathbf{A}_8$ with data in Q1 (blue), Q2 (red), and Q12 (black). The reductions of f_{mud} from 100% to 0% are shown by the darkest color to lightest color. The displayed function are obtained from data set Q12.

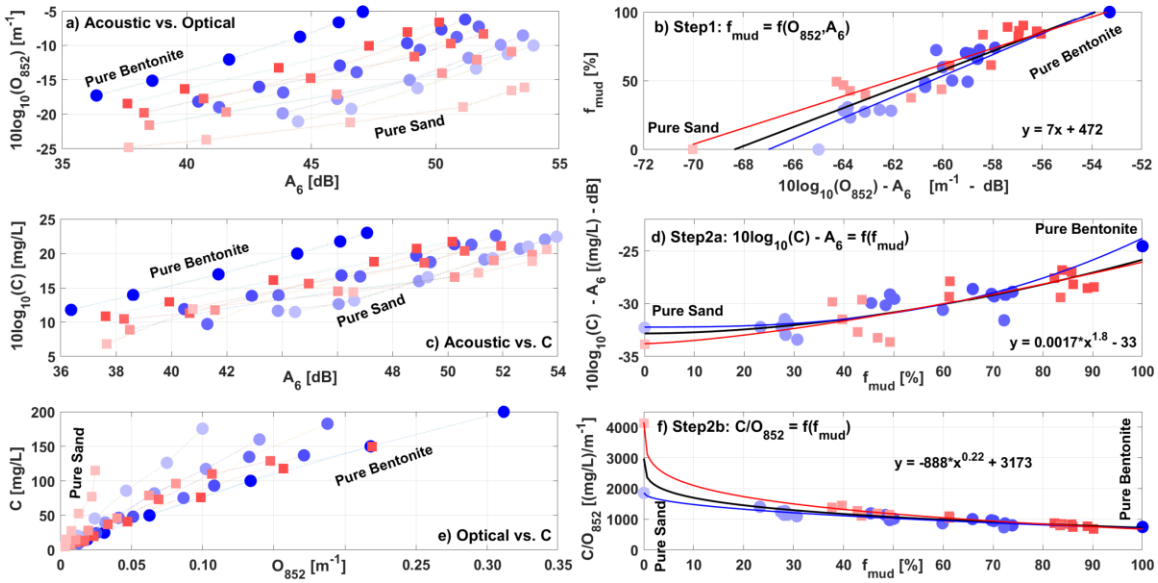

Figure S7. Application of SCI method to the optical/acoustic pair of $\mathbf{O}_{852}$ and $\mathbf{A}_6$ with data in Q1 (blue), Q2 (red), and Q12 (black). The reductions of f_{mud} from 100% to 0% are shown by the darkest color to lightest color. The displayed function are obtained from data set Q12.

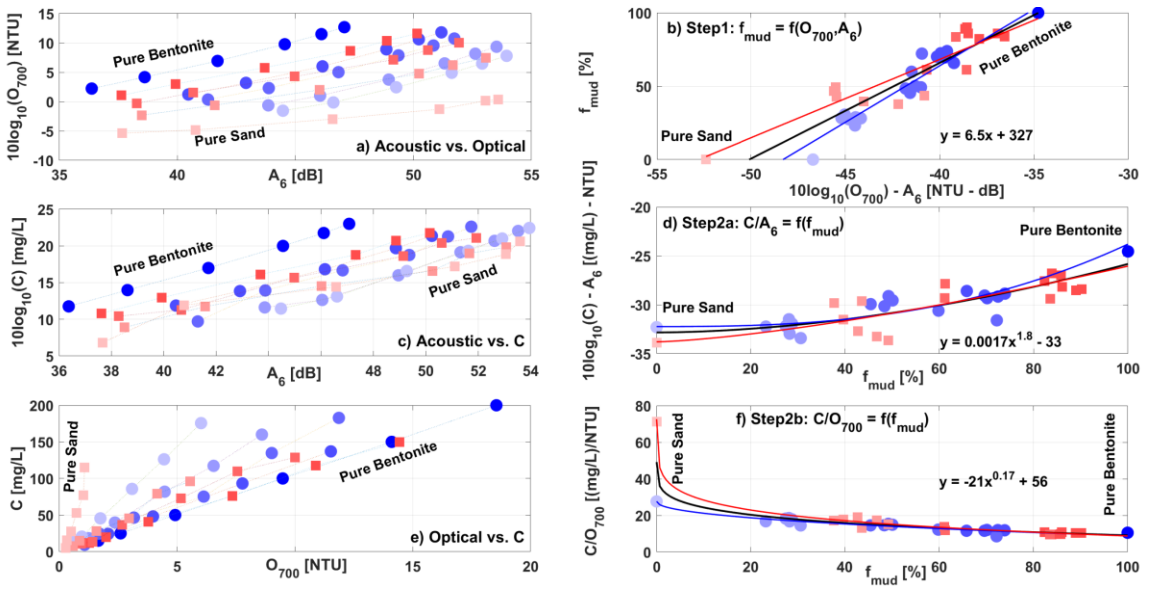

Figure S8. Application of SCI method to the optical/acoustic pair of $\mathbf{O}_{700}$ and $\mathbf{A}_6$ with data in Q1 (blue), Q2 (red), and Q12 (black). The reductions of f_{mud} from 100% to 0% are shown by the darkest color to lightest color. The displayed function are obtained from data set Q12.

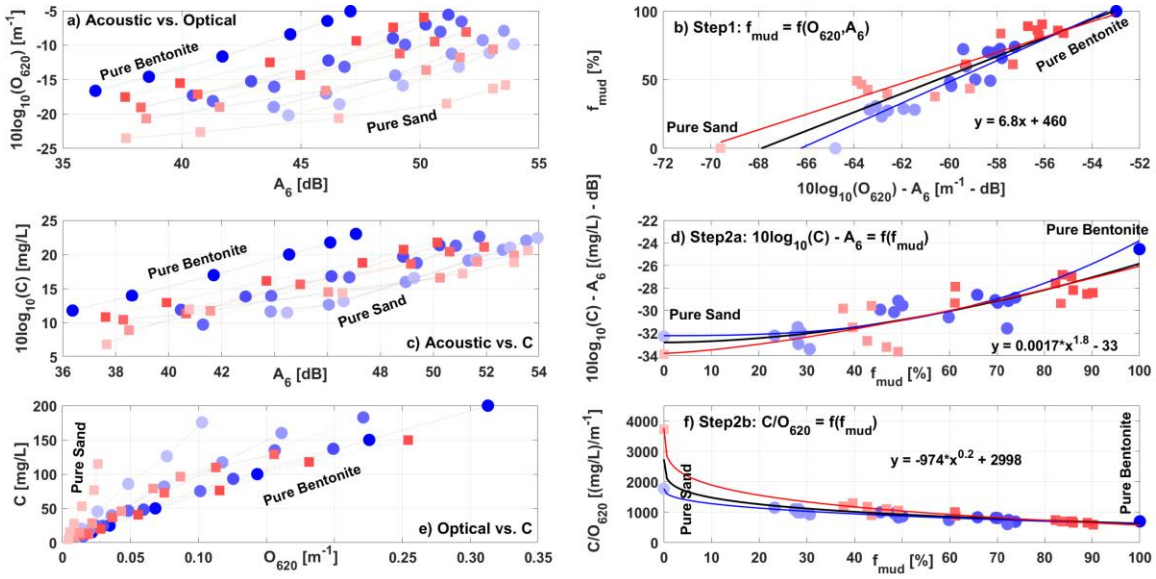

Figure S9. Application of SCI method to the optical/acoustic pair of $\mathbf{O}_{620}$ and $\mathbf{A}_6$ with data in Q1 (blue), Q2 (red), and Q12 (black). The reductions of f_{mud} from 100% to 0% are shown by the darkest color to lightest color. The displayed function are obtained from data set Q12.

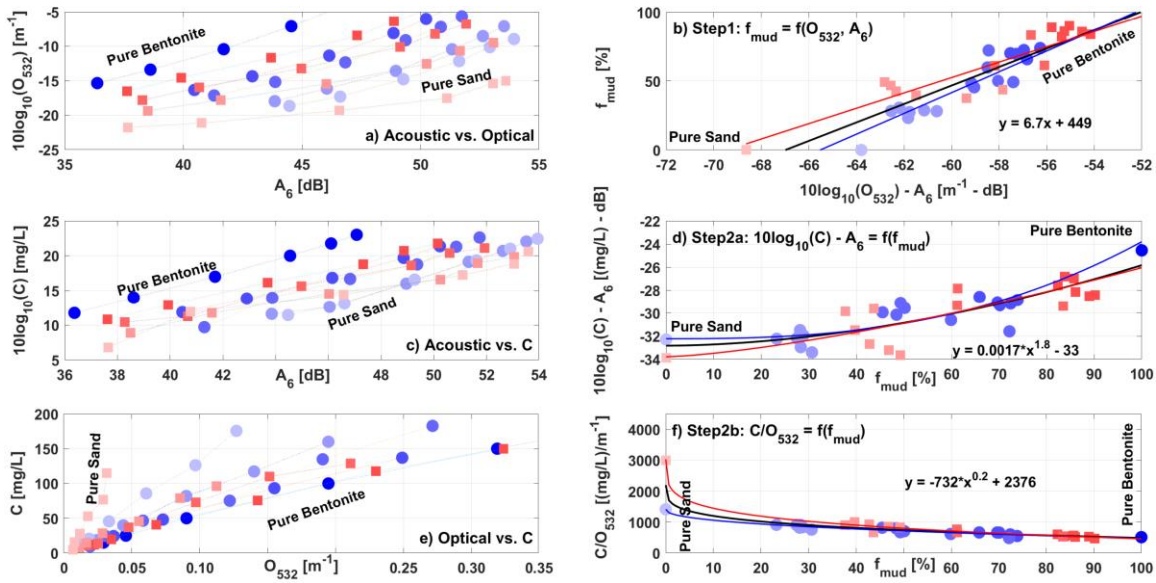

Figure S10. Application of SCI method to the optical/acoustic pair of $\mathbf{O}_{532}$ and $\mathbf{A}_6$ with data in Q1 (blue), Q2 (red), and Q12 (black). The reductions of f_{mud} from 100% to 0% are shown by the darkest color to lightest color. The displayed function are obtained from data set Q12.

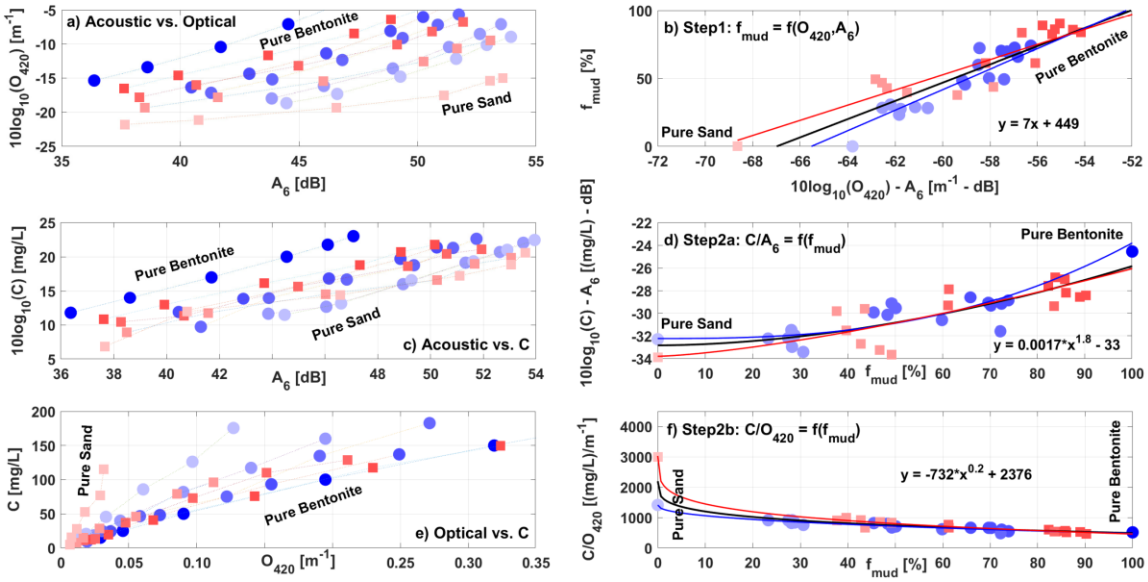

Figure S11. Application of SCI method to the optical/acoustic pair of $\mathbf{O}_{420}$ and $\mathbf{A}_6$ with data in Q1 (blue), Q2 (red), and Q12 (black). The reductions of f_{mud} from 100% to 0% are shown by the darkest color to lightest color. The displayed function are obtained from data set Q12.

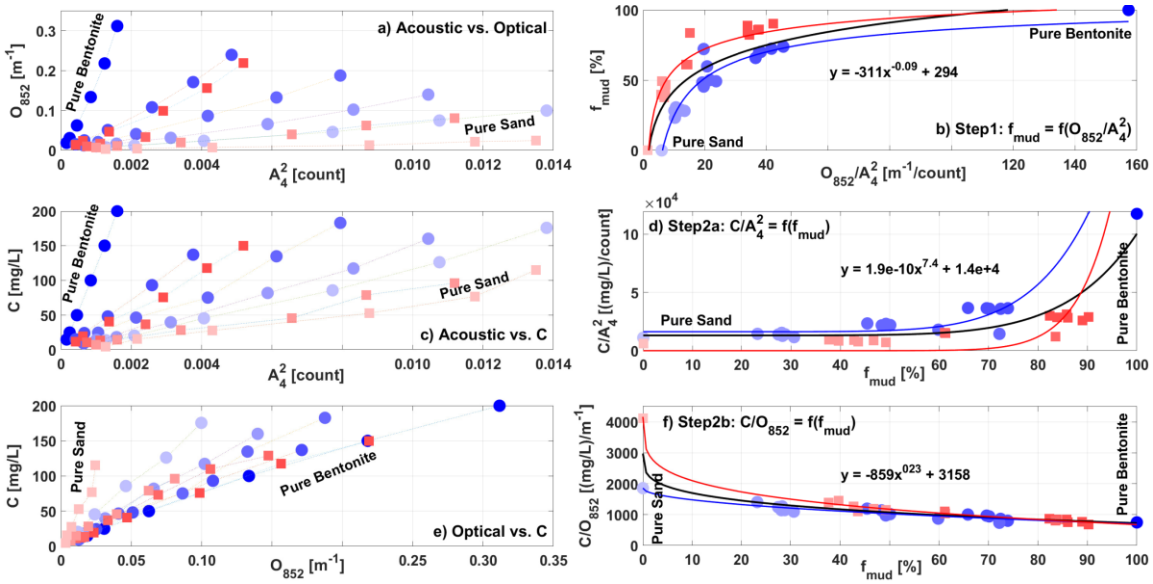

Figure S12. Application of SCI method to the optical/acoustic pair of $\mathbf{O}_{852}$ and $\mathbf{A}_4$ with data in Q1 (blue), Q2 (red), and Q12 (black). The reductions of f_{mud} from 100% to 0% are shown by the darkest color to lightest color. The displayed function are obtained from data set Q12.

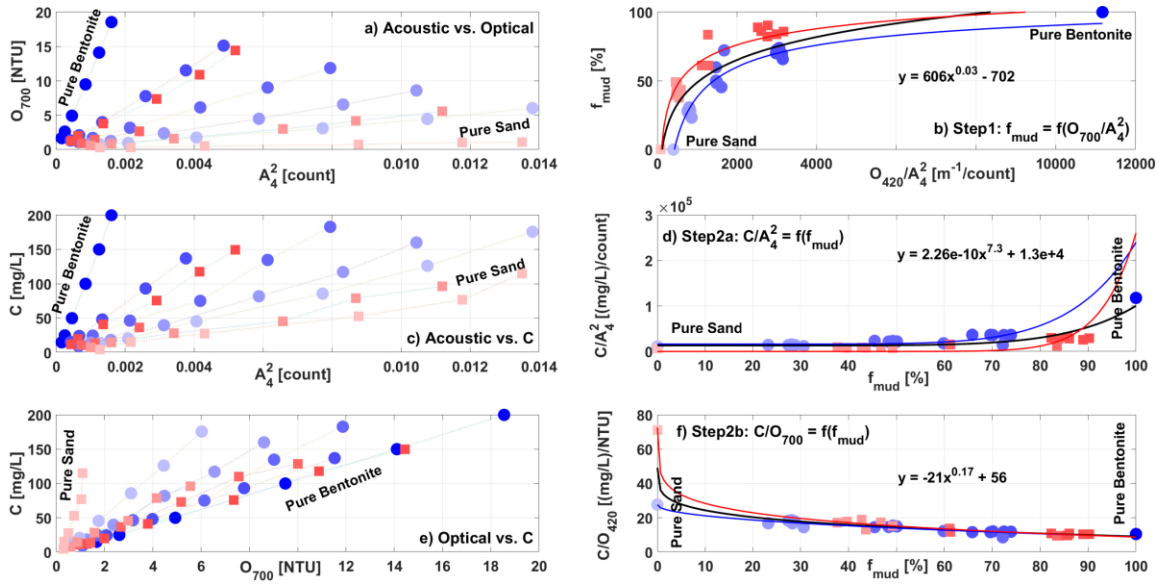

Figure S13. Application of SCI method to the optical/acoustic pair of $\mathbf{O}_{700}$ and $\mathbf{A}_4$ with data in Q1 (blue), Q2 (red), and Q12 (black). The reductions of f_{mud} from 100% to 0% are shown by the darkest color to lightest color. The displayed function are obtained from data set Q12.

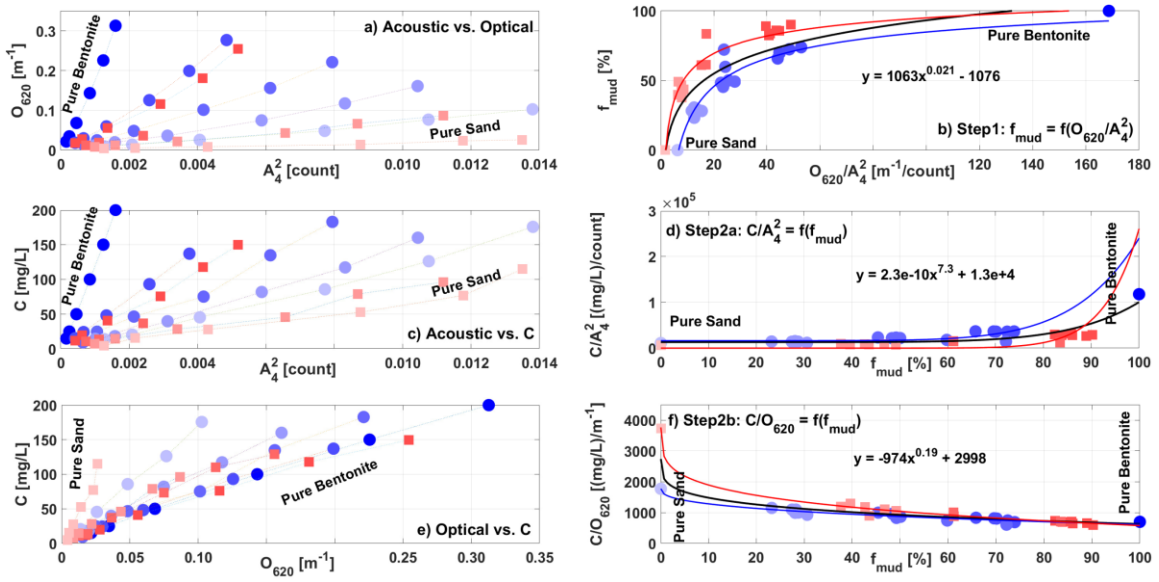

Figure S14. Application of SCI method to the optical/acoustic pair of $\mathbf{O}_{620}$ and $\mathbf{A}_4$ with data in Q1 (blue), Q2 (red), and Q12 (black). The reductions of f_{mud} from 100% to 0% are shown by the darkest color to lightest color. The displayed function are obtained from data set Q12.

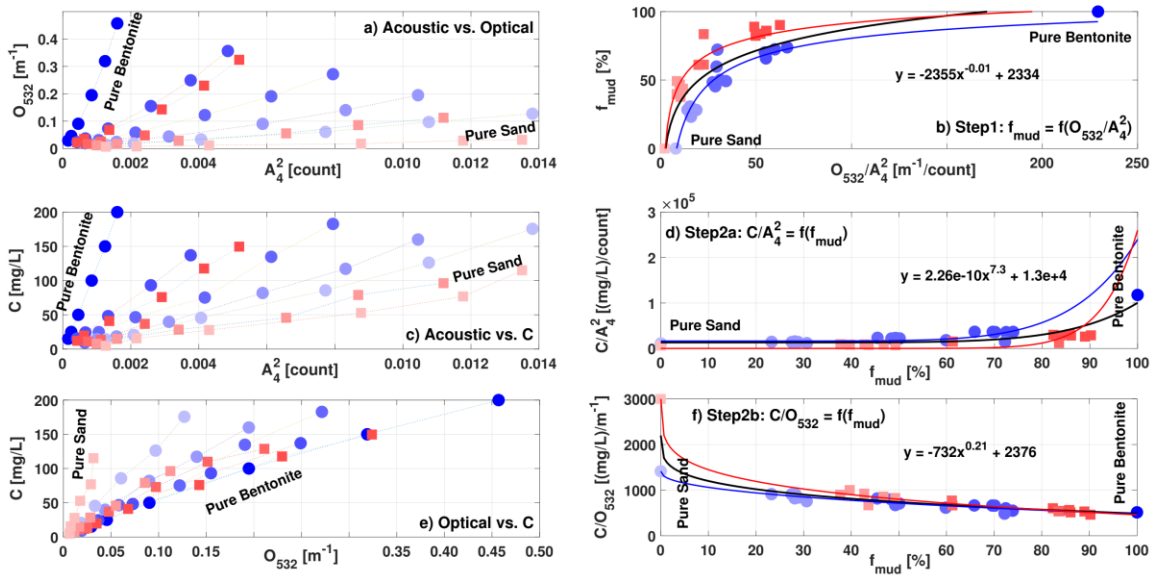

Figure S15. Application of SCI method to the optical/acoustic pair of $\mathbf{O}_{532}$ and $\mathbf{A}_4$ with data in Q1 (blue), Q2 (red), and Q12 (black). The reductions of f_{mud} from 100% to 0% are shown by the darkest color to lightest color. The displayed function are obtained from data set Q12.

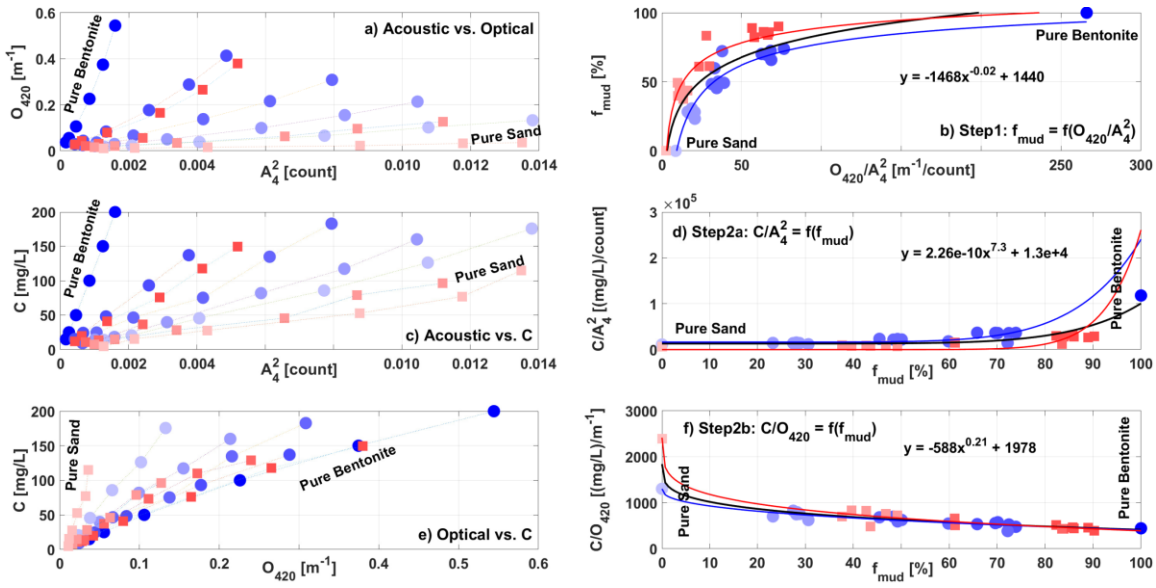

Figure S16. Application of SCI method to the optical/acoustic pair of $\mathbf{O}_{420}$ and $\mathbf{A}_4$ with data in Q1 (blue), Q2 (red), and Q12 (black). The reductions of f_{mud} from 100% to 0% are shown by the darkest color to lightest color. The displayed function are obtained from data set Q12.

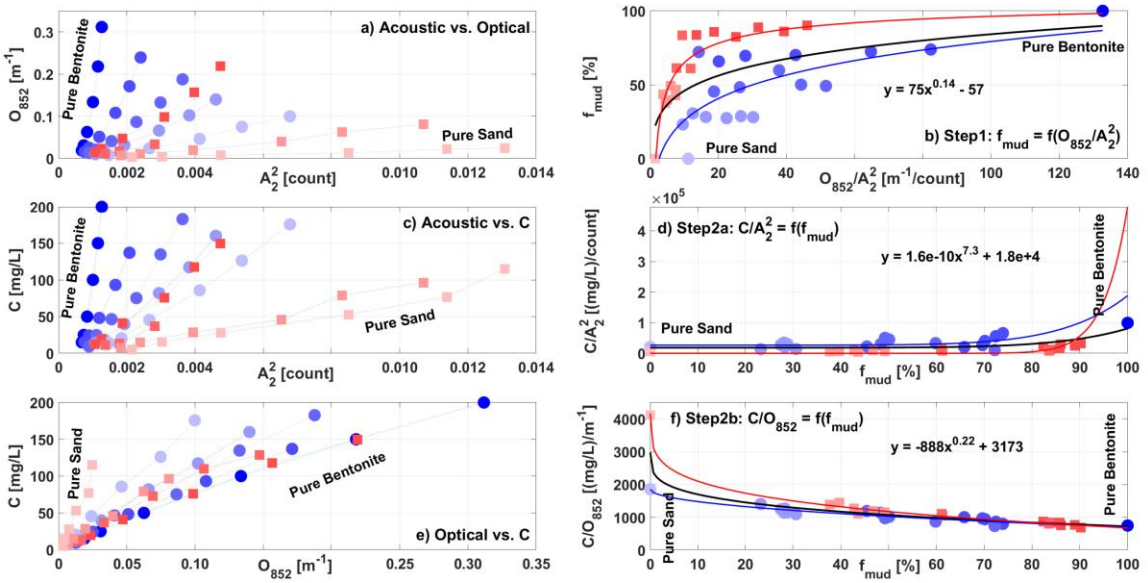

Figure S17. Application of SCI method to the optical/acoustic pair of $\mathbf{O}_{852}$ and $\mathbf{A}_2$ with data in Q1 (blue), Q2 (red), and Q12 (black). The reductions of f_{mud} from 100% to 0% are shown by the darkest color to lightest color. The displayed function are obtained from data set Q12.

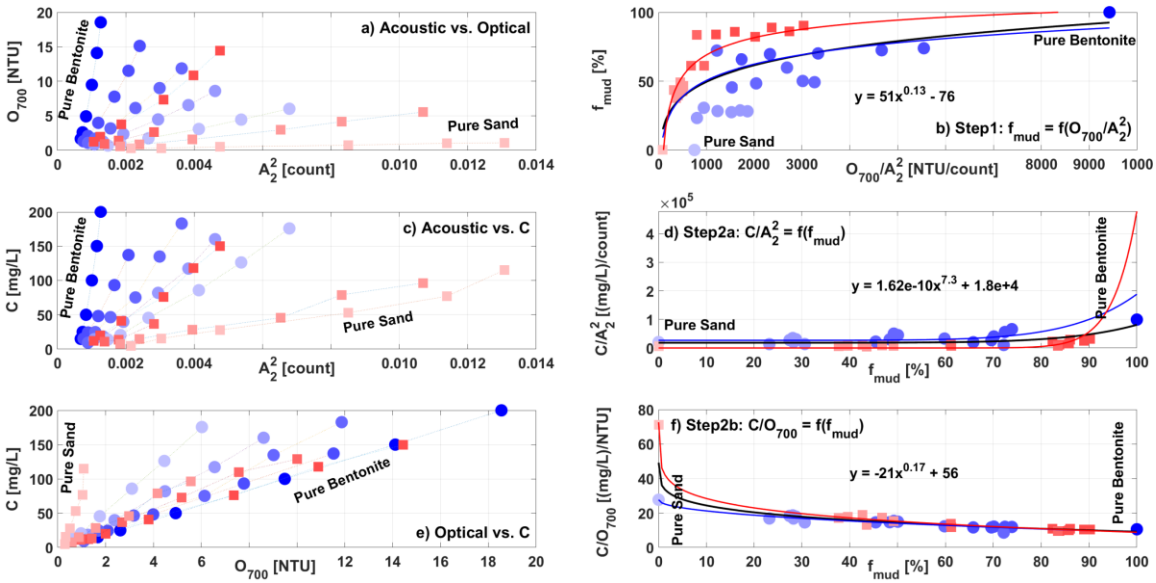

Figure S18. Application of SCI method to the optical/acoustic pair of $\mathbf{O}_{700}$ and $\mathbf{A}_2$ with data in Q1 (blue), Q2 (red), and Q12 (black). The reductions of f_{mud} from 100% to 0% are shown by the darkest color to lightest color. The displayed function are obtained from data set Q12.

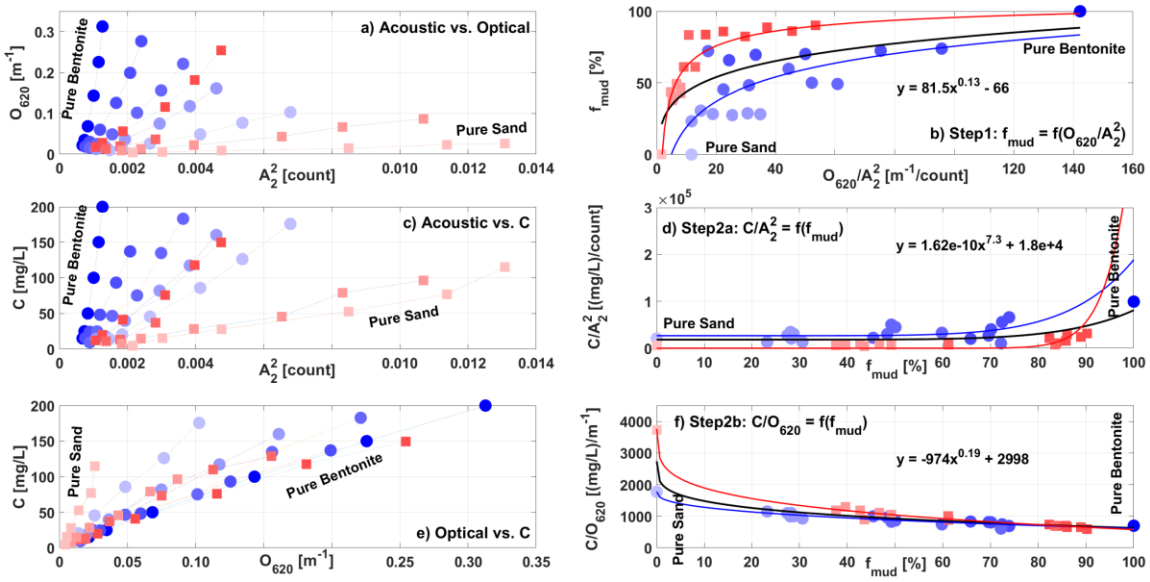

Figure S19. Application of SCI method to the optical/acoustic pair of $\mathbf{O}_{620}$ and $\mathbf{A}_2$ with data in Q1 (blue), Q2 (red), and Q12 (black). The reductions of f_{mud} from 100% to 0% are shown by the darkest color to lightest color. The displayed function are obtained from data set Q12.

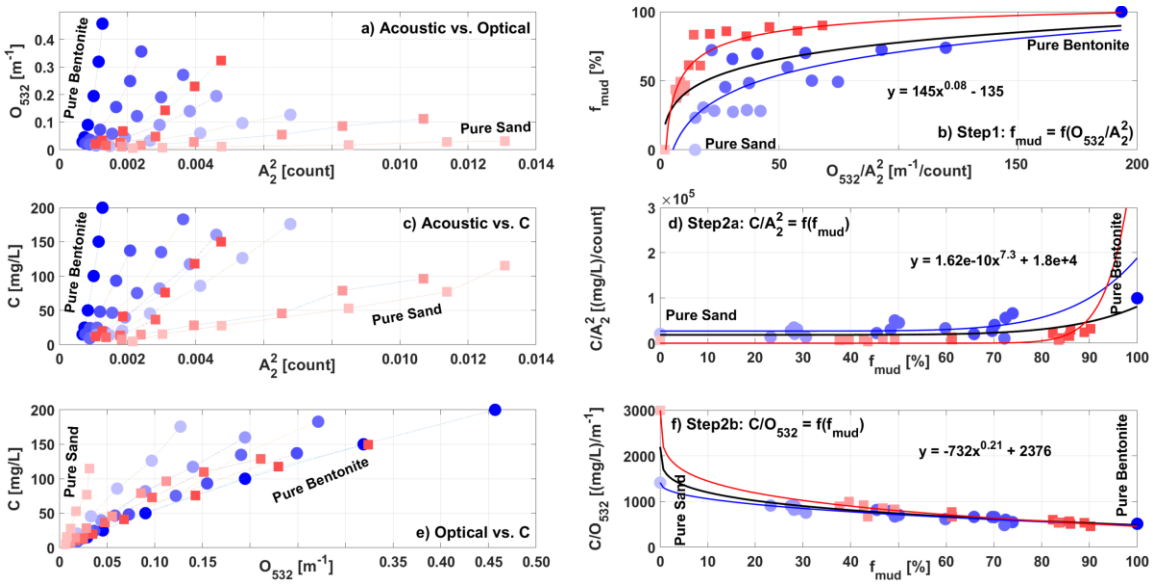

Figure S20. Application of SCI method to the optical/acoustic pair of $\mathbf{O}_{532}$ and $\mathbf{A}_2$ with data in Q1 (blue), Q2 (red), and Q12 (black). The reductions of f_{mud} from 100% to 0% are shown by the darkest color to lightest color. The displayed function are obtained from data set Q12.

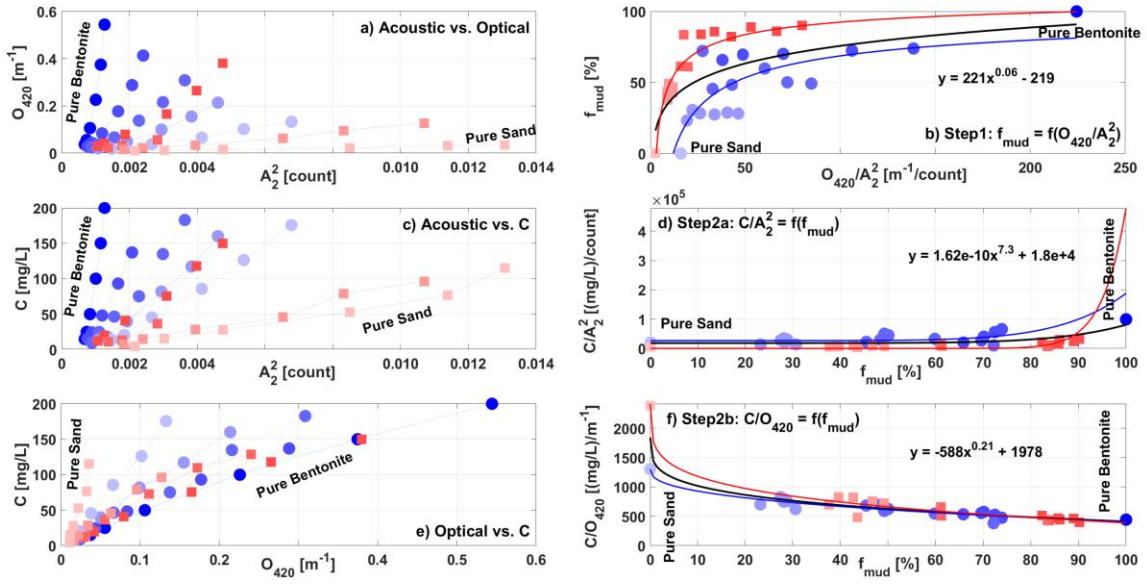

Figure S21. Application of SCI method to the optical/acoustic pair of $\mathbf{O}_{420}$ and $\mathbf{A}_2$ with data in Q1 (blue), Q2 (red), and Q12 (black). The reductions of f_{mud} from 100% to 0% are shown by the darkest color to lightest color. The displayed function are obtained from data set Q12.

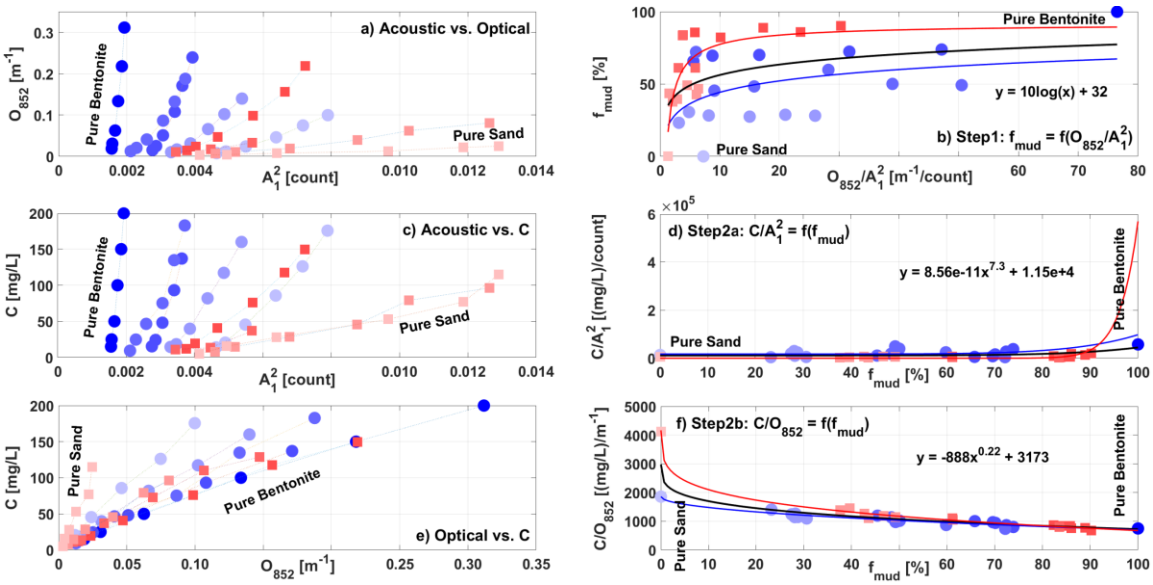

Figure S22. Application of SCI method to the optical/acoustic pair of $\mathbf{O}_{852}$ and $\mathbf{A}_1$ with data in Q1 (blue), Q2 (red), and Q12 (black). The reductions of f_{mud} from 100% to 0% are shown by the darkest color to lightest color. The displayed function are obtained from data set Q12.

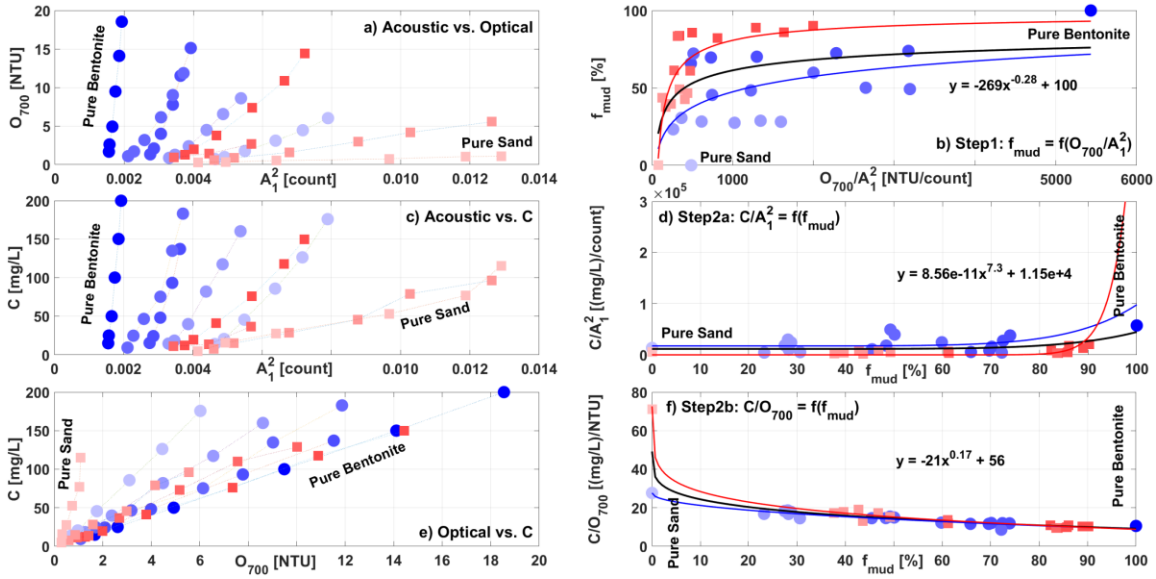

Figure S23. Application of SCI method to the optical/acoustic pair of $\mathbf{O}_{700}$ and $\mathbf{A}_1$ with data in Q1 (blue), Q2 (red), and Q12 (black). The reductions of f_{mud} from 100% to 0% are shown by the darkest color to lightest color. The displayed function are obtained from data set Q12.

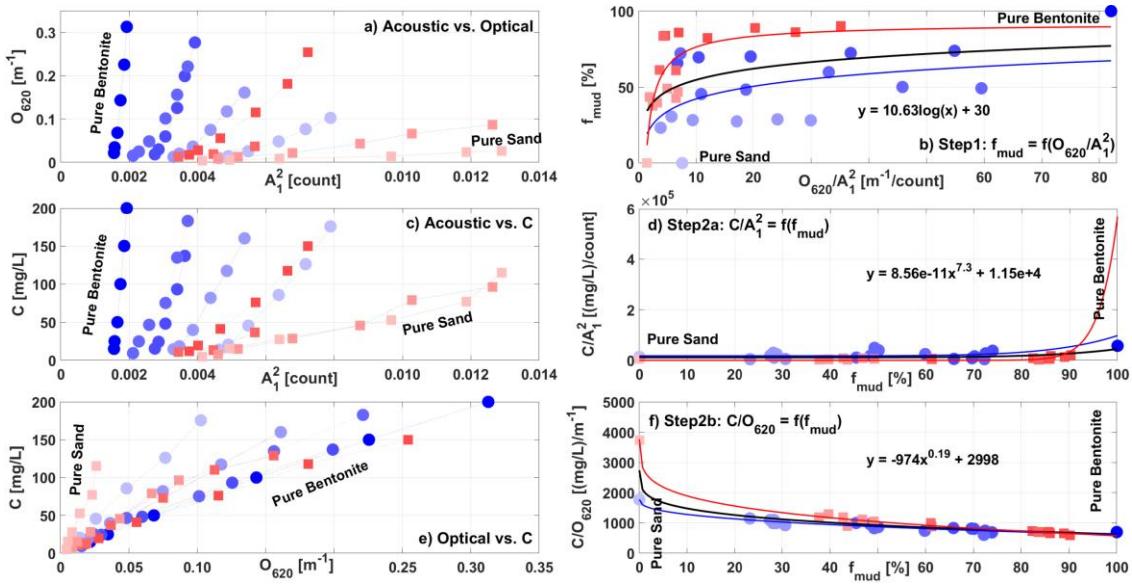

Figure S24. Application of SCI method to the optical/acoustic pair of $\mathbf{O}_{620}$ and $\mathbf{A}_1$ with data in Q1 (blue), Q2 (red), and Q12 (black). The reductions of f_{mud} from 100% to 0% are shown by the darkest color to lightest color. The displayed function are obtained from data set Q12.

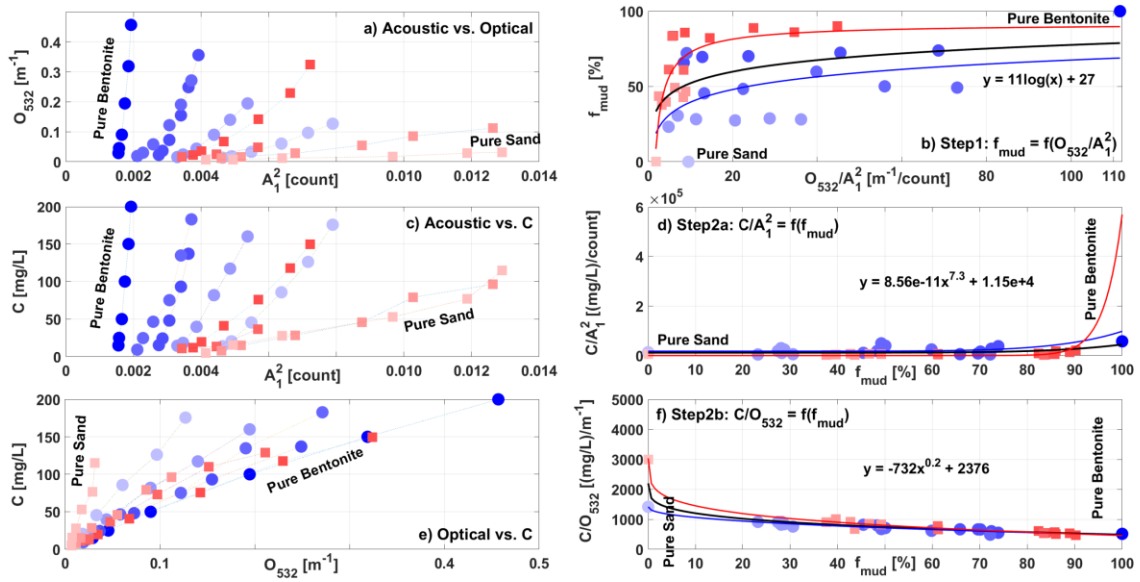

Figure S25. Application of SCI method to the optical/acoustic pair of $\mathbf{O}_{532}$ and $\mathbf{A}_1$ with data in Q1 (blue), Q2 (red), and Q12 (black). The reductions of f_{mud} from 100% to 0% are shown by the darkest color to lightest color. The displayed function are obtained from data set Q12.

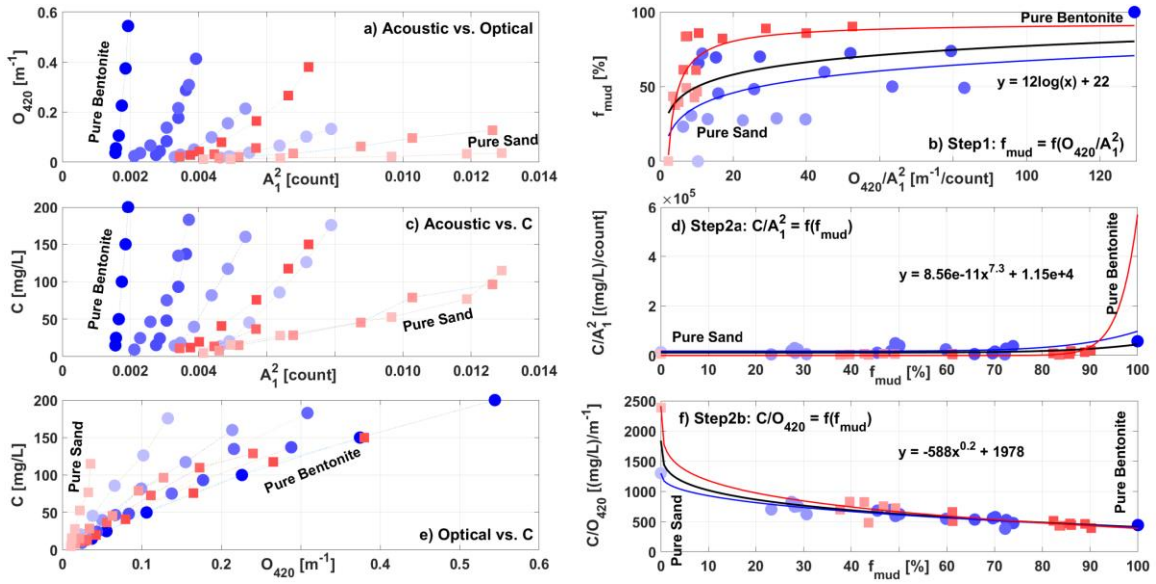

Figure S26. Application of SCI method to the optical/acoustic pair of $\mathbf{O}_{420}$ and $\mathbf{A}_1$ with data in Q1 (blue), Q2 (red), and Q12 (black). The reductions of f_{mud} from 100% to 0% are shown by the darkest color to lightest color. The displayed function are obtained from data set Q12.

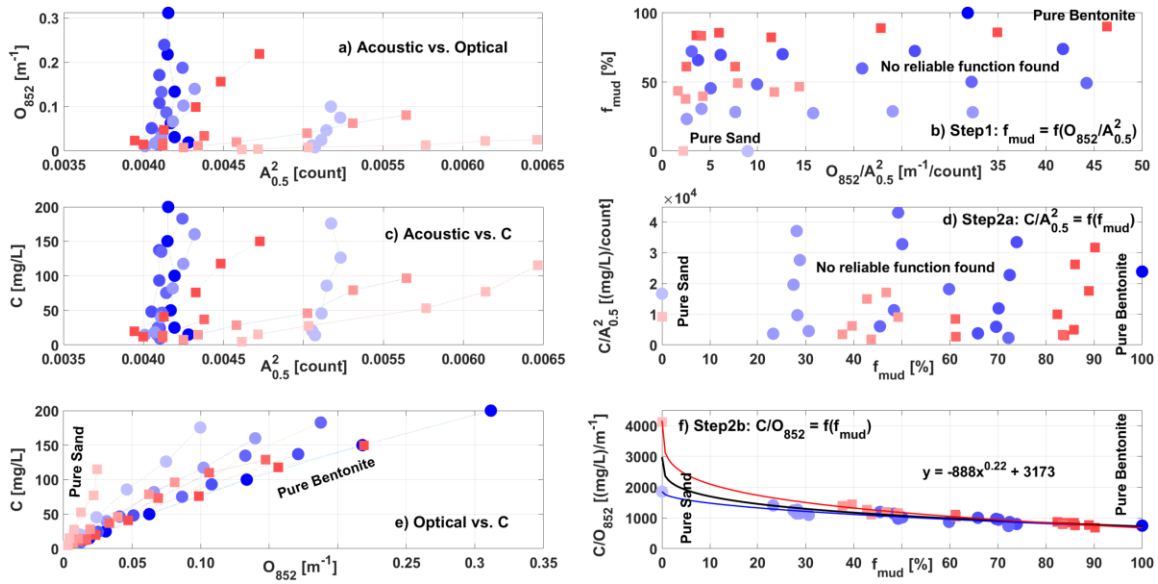

Figure S27. Application of SCI method to the optical/acoustic pair of $\mathbf{O}_{852}$ and $\mathbf{A}_{0.5}$ with data in Q1 (blue), Q2 (red), and Q12 (black). The reductions of f_{mud} from 100% to 0% are shown by the darkest color to lightest color. The displayed function are obtained from data set Q12.

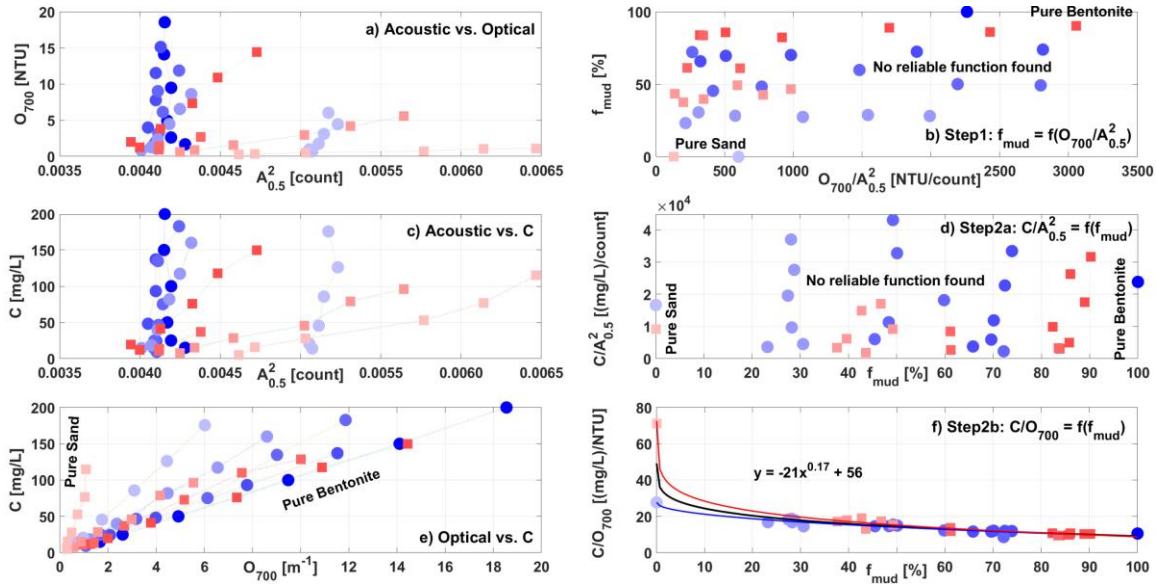

Figure S28. Application of SCI method to the optical/acoustic pair of $\mathbf{O}_{700}$ and $\mathbf{A}_{0.5}$ with data in Q1 (blue), Q2 (red), and Q12 (black). The reductions of f_{mud} from 100% to 0% are shown by the darkest color to lightest color. The displayed function are obtained from data set Q12.

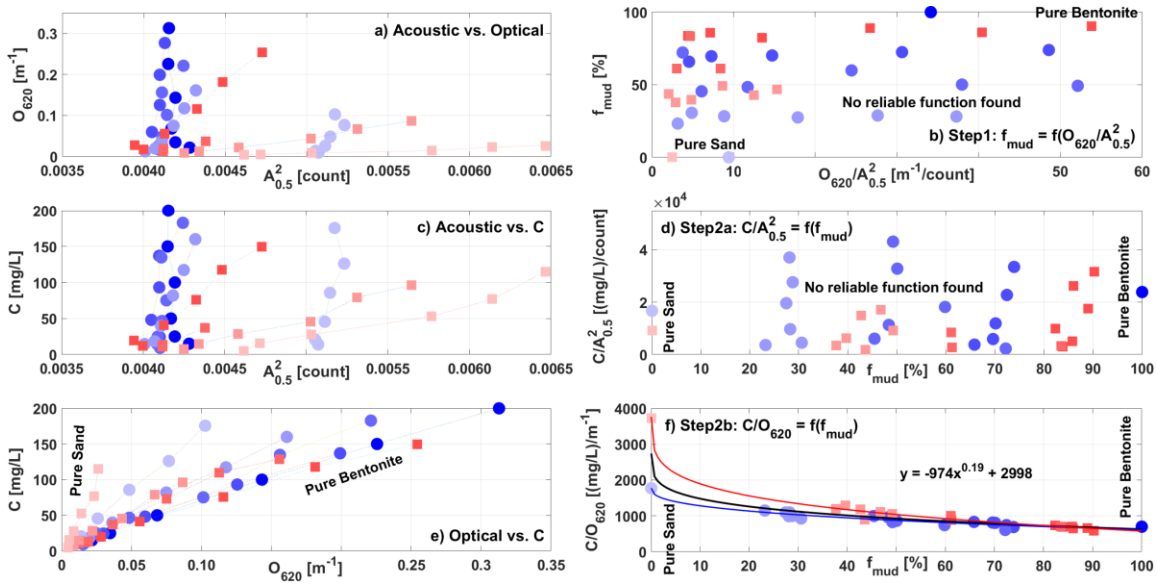

Figure S29. Application of SCI method to the optical/acoustic pair of $\mathbf{O}_{620}$ and $\mathbf{A}_{0.5}$ with data in Q1 (blue), Q2 (red), and Q12 (black). The reductions of f_{mud} from 100% to 0% are shown by the darkest color to lightest color. The displayed function are obtained from data set Q12.

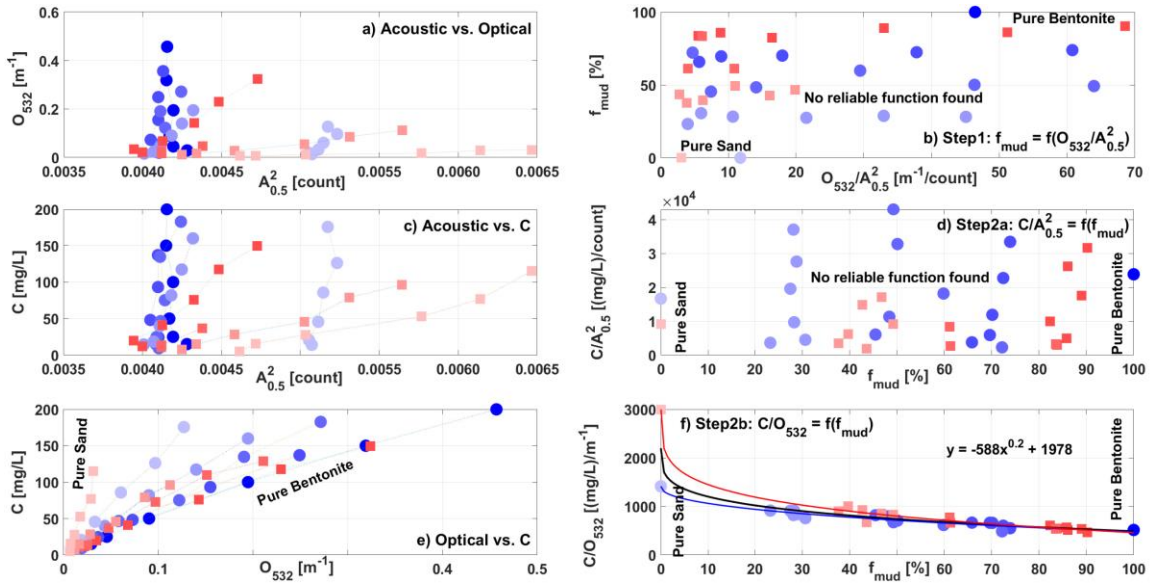

Figure S30. Application of SCI method to the optical/acoustic pair of $\mathbf{O}_{532}$ and $\mathbf{A}_{0.5}$ with data in Q1 (blue), Q2 (red), and Q12 (black). The reductions of f_{mud} from 100% to 0% are shown by the darkest color to lightest color. The displayed function are obtained from data set Q12.

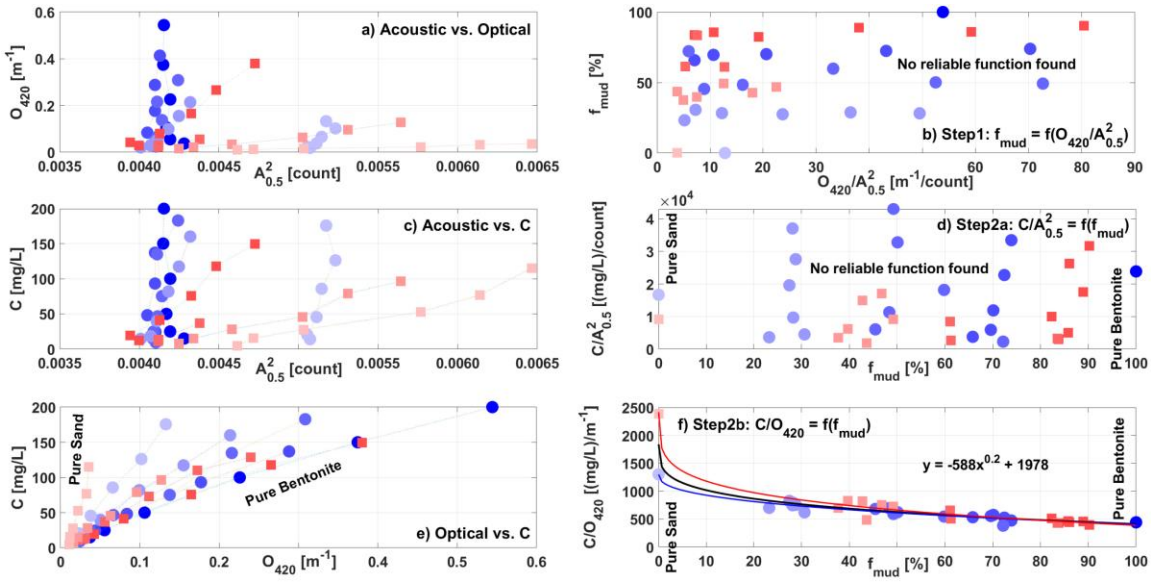

Figure S31. Application of SCI method to the optical/acoustic pair of $\mathbf{O}_{420}$ and $\mathbf{A}_{0.5}$ with data in Q1 (blue), Q2 (red), and Q12 (black). The reductions of f_{mud} from 100% to 0% are shown by the darkest color to lightest color. The displayed function are obtained from data set Q12.